Conducting and permeable states of cell membrane submitted to high voltage pulses: Mathematical and numerical studies validated by the experiments

M. Leguèbe [a,*], A. Silve [b], L.M. Mir [c], C. Poignard [a,*]

[a] Inria Bordeaux, CNRS UMR 5251 & Université de Bordeaux, France
[b] Institute for Pulsed Power and Microwave Technology, Karlsruhe Institute of Technology, Germany
[c] CNRS UMR 8203 & Institut Gustave Roussy, Laboratoire de Vectorologie et Thérapeutiques Anticancéreuses, France

HIGHLIGHTS

- We differentiate conductive and permeable states of a cell membrane.
- We follow concentrations of markers uptaken by permeabilized cells.
- Numerical methods and a 3D code have been specifically written to provide results.
- *in vitro* experimental results validate qualitatively our model.

ARTICLE INFO

ABSTRACT

The aim of this paper is to present a new model of *in vitro* cell electropermeabilization, which describes separately the conducting state and the permeable state of the membrane submitted to high voltage pulses. We first derive the model based on the experimental observations and we present the numerical methods to solve the non-linear partial differential equations. We then present numerical simulations that corroborate qualitatively the experimental data dealing with the uptake of propidium iodide (PI) after millipulses. This tends to justify the validity of our modeling. Forthcoming work will be to calibrate the parameters of the model for quantitative description of the uptake.

© 2014 Elsevier Ltd. All rights reserved.

1. Introduction

Electroporation is a destructuration of a cell membrane organization leading to an increase of permeability to molecules that usually do not diffuse across the membrane. Even though the increase of membrane permeability is a consequence of the electric shock, the internalization of molecules into the cytoplasm cannot be described by the conducting state of the membrane. More precisely, it has been experimentally observed that the cell membrane may remain permeable several minutes after the electric pulses delivery, while experiments by Benz et al. (1979) have reported that the membrane conductivity almost recovers its steady value within several microseconds after the end of the pulse. Therefore it is important, from the modeling point of view, to distinguish the electric phenomenon,

which leads to the increase of membrane conductivity, from the transport of molecules across the permeable membrane. This transport can be obtained by different ways, depending on the molecules: small molecules, which do not interact neither with the membrane nor with the cytoskeleton, can diffuse into the cytoplasm, while active transport (such as ramping process on the membrane or transport due to electrophoretic forces) are needed to make large molecules such as DNA enter the cell.

An electrodiffusion model was already proposed and studied by Smith and Weaver (2012), but it is restricted to the 1D case and the coupling between electroporation and transport across the membrane was not considered. Here we provide a model that describes the *in vitro* process of the internalization of extracellular molecules into the cell, thanks to the application of high amplitude pulses. Our model is based on a non-linear system of partial differential equations, and the numerical results are obtained for 3-dimensional cells.

Even though it is well-known by experimenters that the high conducting state and the high permeable state of the membrane

* Corresponding authors.
E-mail addresses: michael.leguebe@inria.fr (M. Leguèbe),
clair.poignard@inria.fr (C. Poignard).

do not coincide, the current models of electroporation do not distinguish these two states. For instance, the currently most achieved model of DeBruin and Krassowska (1999), Neu and Krassowska (1999, 2006), and Smith et al. (2004) only describes the electrical potential in the cell. Their modeling leads to membrane conducting state, which lasts several seconds (see DeBruin and Krassowska, 1999, Fig. 7). Such a duration is smaller than the permeable state duration observed by experiments with bleomycin – which still enters the cell several minutes after the end of the pulse – but much longer than the duration of the conducting state of the membrane, which stays highly conducting during several microseconds according to Benz et al. (1979). For all these reasons, the current models were not satisfactory. In this paper, we propose a new model, which differentiates the conducting state from the permeable state of the membrane, and we show that the simulations corroborate the experimental data.

The paper is organized as follows. In the next section, we present generically the system of partial differential equations, which will be used to model the cell electropermeabilization. We then clarify the assumptions on which is based the model, and we derive the non-linear law that accounts for the change in the conducting and permeable states of the membrane. We then present numerical methods that make it possible to simulate accurately the electric field and the transport of the molecules from the extracellular domain into the cell cytoplasm. We end by numerical simulations that corroborate qualitatively the different experimental observations.

2. Statement of the generic partial differential equations

In this section, we briefly present the main partial differential equations that describe the phenomenon. Roughly speaking, it consists of a Poisson equation for the electric potential and a diffusion-transport equation for the non-permeant molecules. In Section 3, we will focus on the non-linearity due to the electropermeabilization.

2.1. Geometry, notations

The cytoplasm $\mathcal{O}_c$ and the extracellular medium $\mathcal{O}_e$ are considered as homogeneous materials with respective conductivities (see Fig. 1):

$$\sigma = \begin{cases} \sigma_e & \text{in } \mathcal{O}_e, \\ \sigma_c & \text{in } \mathcal{O}_c. \end{cases}$$

We denote by Γ the boundary of $\mathcal{O}_c$ which is supposed to be smooth. Let $\Omega = \mathcal{O}_e \cup \mathcal{O}_c \cup \Gamma$ be the whole domain, and $\partial\Omega$ its boundary. It is worth noting that Γ is assumed to be fixed and thus
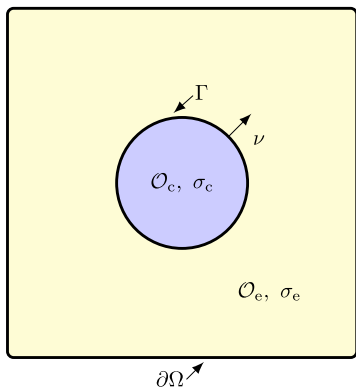
Fig. 1. Scheme of the cell embedded in the extracellular domain.

we do not consider a free-boundary problem. Variations of the volume due to change of osmolarity are not in the scope of the present paper. We refer to Poignard et al. (2011), for more details.

The membrane is thus described by the single interface Γ with no thickness, and ν designates the unit normal vector to Γ, outward from $\mathcal{O}_c$. The flux of a function f across Γ is noted as $\partial_\nu f|_{\Gamma^+}$ or $\partial_\nu f|_{\Gamma^-}$ depending on the side of the interface, respectively $\mathcal{O}_e$ for Γ^+ and $\mathcal{O}_c$ for Γ^-. We use the following notation for the jump of a function f across the interface:

$$[f]_\Gamma = f|_{\Gamma^+} - f|_{\Gamma^-}.$$

2.2. Electric potential

The electric potential is governed by the following equations:

$$\Delta u = 0 \quad \text{in } \mathcal{O}_c \cup \mathcal{O}_e, \tag{1a}$$

$$\sigma_e \partial_\nu u|_{\Gamma^+} = \sigma_c \partial_\nu u|_{\Gamma^-}, \tag{1b}$$

$$C_m \partial_t [u]_\Gamma + S_0([u]_\Gamma - u_0) + S_{ep}(t, [u]_\Gamma)[u]_\Gamma = \sigma_c \partial_\nu u|_{\Gamma^-}, \tag{1c}$$

$$u(t, \cdot)|_{\partial\Omega} = u_{imp}(t, \cdot), \quad u(0, \cdot) = u_0, \tag{1d}$$

where S_0 is the resting membrane conductivity, u_0 is the resting potential and u_{imp} is the boundary condition determined by the pulse. Eq. (1b) corresponds to the continuity of the electric current through the membrane. Eq. (1c) is a Kirchhoff law, where the $C_m \partial_t [u]_\Gamma$ term represents the capacitive effect of the membrane and $S_{ep}(t, [u]_\Gamma)[u]_\Gamma$ is the electroporation current.

The description of the conducting state of the membrane is obtained by imposing a nonlinear law on S_{ep} that will be described in the next section. Note that the term $S_{ep}(t, [u]_\Gamma)[u]_\Gamma$ corresponds to the electroporation current of DeBruin and Krassowska (1999):

$$I_{ep} = N_{ep}(t, [u]_\Gamma) i_{ep}([u]_\Gamma),$$

after linearization of the current through one pore $i_{ep}([u]_\Gamma)$. However, we emphasize that the characteristic time of pore creation of Neu and Krassowska's model depends on the membrane voltage instead of being intrinsic to the membrane. Moreover pore density N_{ep} is not bounded (DeBruin and Krassowska, 1999) which is hardly defensible from the physical point of view, and therefore we prefer to change it into a sliding-door model given in Section 3.

2.3. Diffusion and electric transport of non-permeant molecules

Since the experimental data on electropermeabilization is mainly based on the internalization of non-permeant molecules into cells or vesicles, such as propidium iodide (PI)[1] or DNA, we also describe the motion of these molecules around and inside the cell. This model must take into account the two main modes of propagation of these molecules: the diffusion for small molecules such as PI and the electrophoresis for charged molecules such as DNA. We assume that the electrophoretic forces given by $-\mu_e \nabla u$ holds only in the outer medium, with μ_e being the electrical motility of the molecule M in $\mathcal{O}_e$. This assumption is plausible since the electric field in the cytoplasm is very low due to the shielding effect of the membrane, and since the cytoplasm is composed of cytoskeleton and organelles, which prevents the diffusion and the electric transport of large molecules inside the cell.

We suppose that at the initial time, the concentration of M is constant and equal to M_0 in $\mathcal{O}_e$ while it is set to zero in $\mathcal{O}_c$.

---

[1] PI is a small molecule which is fluorescent inside the cytoplasm of the cell. It is thus a good fluorescent marker of membrane electropermeabilization.

Moreover, according to *in vitro* experiments, the concentration of M on the boundary $\partial\Omega$ of the whole domain Ω is also constant and equals M_0. We denote by d_e and d_c the diffusion constants of the molecule M in $\mathcal{O}_e$ and $\mathcal{O}_c$ respectively. The concentration M in the outer and in the inner media is governed by the following drift–diffusion equation:

$$\partial_t M - d_e \Delta M = \mu_e \nabla \cdot (M\nabla u) \quad \text{in } \mathcal{O}_e,$$
$$\partial_t M - d_c \Delta M = 0 \quad \text{in } \mathcal{O}_c, \tag{2a}$$

with the interface conditions on the membrane

$$d_e \partial_\nu M|_{\Gamma^+} + \mu_e M|_{\Gamma^+} \partial_\nu u|_{\Gamma^+} = d_c \partial_\nu M|_{\Gamma^+}, \tag{2b}$$

$$P_m[M]_\Gamma = d_c \partial_\nu M|_{\Gamma^-}, \tag{2c}$$

$$M|_{t=0} = M_0 \mathbb{1}_{\mathcal{O}_e}, \quad M|_{\partial\Omega} = M_0, \tag{2d}$$

where P_m is the membrane permeability to the considered molecule, and will also be described in the next section. In a similar way as the potential, Eq. (2b) states the flux continuity of M across the membrane. Eq. (2c), that expresses the discontinuity of M across G, is a Kedem–Kachalsky type of transmission conditions (Kargol, 1996).

3. Electro-poration and electro-permeabilization modeling

Modeling both membrane poration and permeabilization consists in deriving equations for the surface membrane conductivity S_{ep} and the membrane permeability P_m respectively.

We split the membrane alteration into two different phenomena that occur with two distinct dynamics: the pore creation, with short-term dynamics, and a long-term permeabilization of the lipid bilayer. This splitting is set to account for two experimental results that seem to be contradictory. On one hand, the observations of Benz et al. (1979) and molecular dynamics (MD) simulations (Tarek, 2005; Tieleman, 2004) show that pores shrink within a few microseconds (even a few nanoseconds for MD simulations) after pulses are off. On the other hand, it has been reported that the permeable state lasts several minutes after the pulse delivery (Rols et al., 1998; Teissié and Ramos, 1998). Therefore we differentiate the porated state from the permeabilized state, describing the local degree of poration by X_1, and the degree of permeabilization by X_2. The effective porosity and the permeability of cell membranes have never been measured, unlike for soils as referred by Chapuis and Aubertin (2003). Actually, the underlying mechanisms of the phenomena and the link between porosity and permeability have not been explained yet, as described in Section 5.5 of Silve et al. (2014). We thus choose to refer to X_1 and X_2 as degrees of porosity and permeability respectively, in order to distinguish between the standard porosity and the permeability of soils.

We associate with each state a specific membrane conductivity and membrane permeability:

- S_0 and P_0 are the respective membrane conductivity and permeability to the molecule M at rest.
- S_1 and P_1 are the constants that represent the membrane conductivity and the membrane permeability to M of a fully porated region of the membrane.
- S_2 and P_2 are the membrane conductivity and the membrane permeability to M of the altered lipid bilayer.

The total surface conductivity and permeability of the membrane are then set as

$$S_m(t,s) = S_0 + S_{ep}(t,s) = S_0 + X_1(t,s)S_1 + X_2(t,s)S_2, \quad \forall t > 0, \ s \in \Gamma, \tag{3}$$

$$P_m(t,s) = P_0 + X_1(t,s)P_1 + X_2(t,s)P_2, \quad \forall t > 0, \ s \in \Gamma. \tag{4}$$

Let us emphasize the main difference between the membrane conductivity S_m, which is an intrinsic property of the membrane, and P_m, which is the membrane permeability to a specific molecule.

The order of magnitude of S_1 is much larger than the resting conductivity S_0 as shown in experiments of Benz et al. (1979). Since these observations highlight a remaining conductivity after pulse delivery which is slightly above the resting conductivity, the value S_2 is set so as

$$S_0 < S_2 \ll S_1.$$

Permeabilization constants are taken in the same way:

$$P_0 < P_2 \ll P_1,$$

since it is theoretically much easier for a molecule to enter the cytoplasm *via* a pore rather than through a permeable but non-porated membrane.

Remark 3.1 (*A membrane can be simultaneously permeable and not conducting.*). The relation between porosity and permeability has been extensively studied for soils. We refer for instance to Chapuis and Aubertin (2003). Note that for cell membranes, it is very difficult to link porosity and permeability thanks to an algebraic equation as in Chapuis and Aubertin (2003). Actually, since the conducting state of the membrane lasts several microseconds while the permeable state lasts several minutes, porosity and permeability should be linked in a very complex way which is not addressed in this paper. It is also worth noting that pore size of DNA cannot last several minutes otherwise the cell integrity should be altered, while few minutes after the electric shock, DNA can be uptaken by the cells. This means that there is another mechanism thanks to which large molecules cross the membrane. Therefore, in the present paper we consider porated and permeable states separately. Here is the important feature of our modeling: even without any pore, a membrane, which has been fragilized or destructured by the electric pulse, has a non-zero permeability, and thus may let molecules enter into the cytoplasm, even though its conductivity is low.

Remark 3.2 (*Membrane conductivity is intrinsic, not its permeability*). Note that if the conductivities (S_0, S_1, S_2) are intrinsic to the cell, the permeabilities (P_0, P_1, P_2) depend on the molecules that cross the membrane, in particular on their molecular weight, spatial conformation and electric charge. For example, if a non-permeant molecule such as bleomycin or DNA is considered, the minimum value of permeability is set to $P_0 = 0$.

We will now focus on the description of the degree of poration X_1 in Section 3.1 and we then describe the degree of permeabilization X_2 in Section 3.2.

3.1. Pore creation and pore resealing

The function X_1 describes the degree of porosity of the membrane. It is related to the high conducting state of the membrane as reported by the experiments of Benz et al. (1979). It satisfies a differential equation similar to a *sliding-door* model of electrophysiology. As pores are created only if a threshold voltage is overcome, we set

$$\partial_t X_1 = F_1(X_1, [u]), \tag{5}$$

with the initial condition

$$X_1(t=0, s) = X_1^0.$$
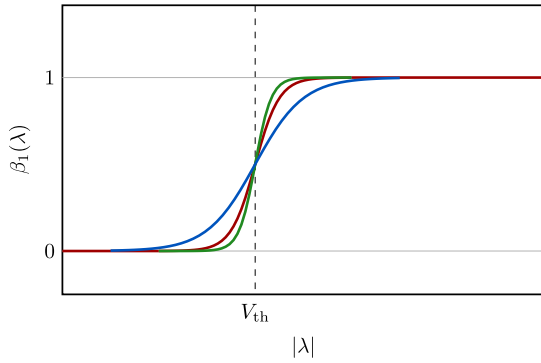
Fig. 2. The function β_1 for different slope values k_1.

The function F_1 is a function of the transmembrane potential difference $[u]$ and of X_1 itself given by

$$F_1(X_1, [u]) = \frac{\beta_1([u]) - X_1}{\tau_1}, \qquad (6)$$

where τ_1 is the characteristic time of the poration process and β_1 is given by

$$\beta_1(\lambda) := \frac{1 + \tanh(k_1(|\lambda| - V_{th}))}{2}, \qquad (7)$$

where k_1 describes the slope of the sigmoidal function and V_{th} the threshold voltage above which electroporation occurs (see Fig. 2).

3.2. Membrane permeabilization: a reaction–diffusion model for lipid alteration

Consider now the degree of permeabilization X_2. The model of membrane permeabilization is based on the following assumptions, which come from experimental observations:

- We hypothesize that permeabilization results of a long-term effect of defects in the membrane related to an alteration of phospholipids due to the presence of water inside the membrane. We thus use X_1 as an initiating factor of permeabilization. Actually it has been reported by Harakawa et al. (2005) and Nikolova et al. (2012) that electric field changes the phospholipid composition, by altering the lipid property.
- The dynamics of alteration and reconstruction of the membrane are dramatically not the same as it has been observed by the experiments (Rols et al., 1998; Teissié and Ramos, 1998). The alteration of the lipids is a physical phenomenon, which occurs as long as pores are present on the membrane and whose characteristic time is in the order of the microsecond. On the contrary, the membrane recovery is a biological phenomenon, called exocytosis, which takes time: it happens for minutes after the electric shock. Thus, we introduce two different time constants: $\tau_{2,perm}$ for the permeabilization and $\tau_{2,res}$ for the membrane recovery due to exocytosis, $\tau_{2,res}$ being in the order of one hour as reported by Glogauer et al. (1993).
- Lipids diffuse along the membrane at a speed d_L around $1 \, \mu m^2/s$ (Chen et al., 2006; Vaz et al., 1984; Tocanne et al., 1994), which is non-negligible compared to the lapse of time between two pulses (usually of the order of 1 s), and therefore this surface diffusion has to be accounted for.

We thus use a reaction–diffusion equation to describe the degree of lipid alteration X_2:

$$\partial_t X_2 - d_L \Delta_\Gamma X_2 = F_2(X_1, X_2) \quad \text{on } \Gamma, \qquad (8a)$$

with the initial condition

$$X_2(t = 0, s) = X_2^0. \qquad (8b)$$

We set

$$F_2(X_1, X_2) = \begin{cases} \dfrac{\beta_2(X_1) - X_2}{\tau_{2,perm}} & \text{if } \beta_2(X_1) - X_2 \geq 0, \\[2mm] \dfrac{\beta_2(X_1) - X_2}{\tau_{2,res}} & \text{if } BT(X_1) - X_2 \leq 0, \end{cases} \qquad (9)$$

with

$$\beta_2(\lambda) := \frac{1 + \tanh(k_2(|\lambda| - X_{1,th}))}{2}, \qquad (10)$$

where $X_{1,th}$ is a poration threshold. Since F_2 is a Lipschitz function with respect to its first variable, it is clear that existence and uniqueness for X_2 holds for any X_1 smooth enough, and X_2 is also Lipschitz in X_1. The mathematical analysis of the whole model is not in the scope of this paper and we are confident that it can be obtained thanks to quite standard analysis. However, from the modeling point of view it is important to verify that X_2 is actually a degree of permeabilization, meaning that, similarly to X_1, it takes values in $[0, 1]$. The following proposition ensures this property.

Proposition 3.3 (*Boundedness of X_2*). *Let X_2 be the solution to* (8). *Then for almost any $(t, s) \in (0, T) \times \Gamma$*

$$0 \leq X_2(t, s) \leq 1.$$

Proof. Let us define $X_2^- := \max(0, -X_2)$. Multiplying (12k) by X_2^- and integrating by part lead to

$$\frac{1}{2} \frac{d}{dt} \|X_2^-\|_{L^2(\Gamma)}^2 + d_L \|\nabla X_2^-\|_{L^2(\Gamma)}^2 = -\int_\Gamma F(X_2, X_1) X_2^- \, ds,$$

but since

$$F(X_2, X_1) X_2^- = \frac{\beta_2(X_1) - X_2}{\tau_{2,perm}} X_2^- \geq 0,$$

and since $\|X_2^-\|^2|_{t=0} = 0$ we infer that X_2 is positive. Defining $Y_2 = X_2 - 1$, introducing similarly $Y_2^+ := \max(0, X_2 - 1)$, and using the fact that

$$F_2(Y_2 + 1, X_1) = \begin{cases} \dfrac{\beta_2(X_1) - 1 - Y_2}{\tau_{2,perm}} & \text{if } \beta_2(X_1) - 1 - Y_2 \geq 0, \\[2mm] \dfrac{\beta_2(X_1) - 1 - Y_2}{\tau_{2,res}} & \text{if } \beta_2(X_1) - 1 - Y_2 \leq 0, \end{cases} \qquad (11)$$

and thus

$$F(Y_2 + 1, X_1) Y_2^+ = \frac{\beta_2(X_1) - 1 - X_2}{\tau_{2,res}} Y_2^+ \leq 0,$$

show that Y_2^+ equals zero and thus $X_2 \leq 1$. □

Remark 3.4 (*The choice of the sigmoidal function*). For both poration and permeabilization degrees, we used hyperbolic tangents to describe the change in the membrane properties (7)–(10): the functions β_1 and β_2 are defined thanks to two parameters describing a threshold and a speed of the switch between these states. Note that any (smooth enough) sigmoidal function involving similar parameters can be used in the model. In particular, if one wants to relate the degree of poration to the local electrostatic energy, one can use for example:

$$\beta_1(\lambda) = e^{-k(V/\lambda)^2},$$

with V and k being the new threshold and switch speed parameters respectively. However, the hyperbolic tangent has the advantage to identify easily the threshold value and the speed of switch between the non-porated (resp. the non-permeabilized state) state and the porated state (resp. the permeabilized state).

4. Numerical methods

Before presenting the numerical methods, let us summarize the complete model of conducting and permeable states of membrane:

$$\Delta u = 0 \quad \text{in } \mathcal{O}_c \cup \mathcal{O}_e, \tag{12a}$$

$$\partial_t M - d_e \Delta M = \mu_e \nabla \cdot (M \nabla u) \quad \text{in } \mathcal{O}_e, \tag{12b}$$

$$\partial_t M - d_c \Delta M = 0 \quad \text{in } \mathcal{O}_c, \tag{12c}$$

with the transmission conditions

$$\sigma_e \partial_\nu u|_{\Gamma^+} = \sigma_c \partial_\nu u|_{\Gamma^-}, \tag{12d}$$

$$C_m \partial_t [u]_\Gamma + S_0([u]_\Gamma - u_0) + S_{ep}(t, [u]_\Gamma)[u]_\Gamma = \sigma_c \partial_\nu u|_{\Gamma^-}, \tag{12e}$$

$$d_e \partial_\nu M|_{\Gamma^+} + \mu_e M|_{\Gamma^+} \partial_\nu u|_{\Gamma^+} = d_c \partial_\nu M|_{\Gamma^+}, \tag{12f}$$

$$P_m(t, [u]_\Gamma)[M]_\Gamma = d_c \partial_\nu M|_{\Gamma^-}, \tag{12g}$$

where

$$S_{ep}(t, [u]_\Gamma) = X_1(t, [u]_\Gamma)S_1 + X_2(t, [u]_\Gamma)S_2, \tag{12h}$$

$$P_m(t, [u]_\Gamma) = X_1(t, [u]_\Gamma)P_1 + X_2(t, [u]_\Gamma)P_2, \tag{12i}$$

with

$$\partial_t X_1 = F_1(X_1, [u]), \tag{12j}$$

$$\partial_t X_2 - d_L \Delta_\Gamma X_2 = F_2(X_1, X_2), \tag{12k}$$

with the boundary conditions

$$u|_{\partial\Omega} = u_{imp}(t), \quad M|_{\partial\Omega} = M_0, \tag{12l}$$

and with the initial conditions

$$u(0, \cdot) = u_0, \quad M(0, \cdot) = M^0 \mathbb{1}_{\mathcal{O}_e}, \quad X_1(0, \cdot) = 0, \quad X_2(0, \cdot) = 0. \tag{12m}$$

4.1. Discretization of equations in extra- and intracellular domains

In order to solve numerically the complete model (12), several discretization methods are needed. The equations on the electric potential u (12a), (12d) and (12e) are solved using the same numerical scheme as already used in the previous paper dedicated to the electric part of the model (Kavian et al., 2014). We also described precisely the method in Leguèbe et al. (2013). The scheme is based on finite differences on a cartesian grid, with a special treatment of discontinuities at an interface. Its main feature is to insert two additional unknowns per intersection between the interface and the cartesian grid. These unknowns make it possible to compute quantities that are defined on the membrane only, such as $[u]$, S_{ep} and P_m. This method is of order 2 in space and order 1 in time. It has been adapted to the 3-dimensional case for the simulations that will be presented in Section 5.

In order to avoid confusion between the indexation systems that will be described, we will index cartesian grid points by $\mathbf{i}$, which is a 3-uple: $\mathbf{i} \in \mathbb{N}^3$, while the intersection points between the grid and the interface are denoted by $j \in \mathbb{N}$. Let $\tilde{\Gamma}$ denote the set of these intersection points.

When necessary, we make the distinction between values inside and outside the cell using the superscripts c and e: u^c and u^e denote the potential respectively inside and outside the cell. $(\Delta u)_{\mathbf{i}}^n$ and $(\partial_\nu u^c)_j^n$, $(\partial_\nu u^e)_j^n$ designate respectively the discretizations of the Laplacian of u at the grid point $P_{\mathbf{i}}$ and the normal derivative of u^c, u^e at the point P_j of the interface at the time iteration $t^n = n\delta t$ (δt being the time pace). The numerical scheme for the potential

equations is the following:

$$\forall \mathbf{i} \in [0, N]^3, \quad (\Delta u)_{\mathbf{i}}^{n+1} = 0, \tag{13a}$$

$$\forall P_j \in \tilde{\Gamma}, \quad \sigma_c(\partial_\nu u^c)_j^{n+1} - \sigma_e(\partial_\nu u^e)_j^{n+1} = 0, \tag{13b}$$

$$\forall P_j \in \tilde{\Gamma}, \quad \frac{C_m}{\delta t}(u_j^{e,n+1} - u_j^{c,n+1}) - \sigma_e(\partial_\nu u^e)_j^{n+1}$$
$$= \left(\frac{C_m}{\delta t} + S_m^n\right)(u_j^{e,n} - u_j^{c,n}), \tag{13c}$$

where N is the number of grid discretization points. A Dirichlet boundary condition in a given direction, coupled with an isolating Neumann condition in the other directions, simulates an external uniform electric field around the cell.

Since it is based on the same geometry as the potential, the model of transport and diffusion of molecules is solved with the same discretization method for the Laplacian on $\mathcal{O}_e$ and $\mathcal{O}_c$, and for the normal derivatives on Γ. However, since the position of the interface (typically a sphere) in a cartesian grid leads to large irregularities, the method is too restrictive on the time pace to solve Eqs. (12b), (12c), (12f) and (12g) in a single iteration.

We decided to split the transport and diffusion steps as follows: let $\mathbf{E}^n$ be the electric field computed from u^n:

$$\forall \mathbf{i} \in [0, N]^3, \quad \frac{1}{\delta t} M_{\mathbf{i}}^* = \frac{1}{\delta t} M_{\mathbf{i}}^n + (\nabla \cdot (\mu M \mathbf{E}^n))_{\mathbf{i}}^n, \tag{14a}$$

$$\forall P_j \in \tilde{\Gamma}, \quad \begin{cases} \partial_\nu M_j^* = 0 & \text{if } \mathbf{E}^n \cdot \boldsymbol{\nu} > 0, \\ M_j^{c,*} = M_j^{e,*} & \text{if } \mathbf{E}^n \cdot \boldsymbol{\nu} < 0, \end{cases} \tag{14b}$$

where $(\nabla \cdot (\mu M \mathbf{E}^n))_{\mathbf{i}}^n$ is the discretization of $\nabla \cdot (\mu M \mathbf{E})$ at $P_{\mathbf{i}}$ at the time t^n using an order 1 upwind scheme, and $\boldsymbol{\nu}$ is the outward unit normal vector to the interface. Note that the motility μ vanishes if the point $P_{\mathbf{i}}$ is inside the cell. The Dirichlet boundary condition equal to M^0 is used if the electric field is entering the simulation box, that is, when $\nabla u \cdot \boldsymbol{\nu} \geq 0$ on $\partial\Omega$.

The diffusion step is discretized as follows:

$$\forall \mathbf{i} \in [0, N]^3, \quad \frac{1}{\delta t} M_{\mathbf{i}}^{n+1} - d(\Delta M)_{\mathbf{i}}^{n+1} = \frac{1}{\delta t} M_{\mathbf{i}}^n, \tag{15a}$$

$$\forall P_j \in \tilde{\Gamma}, \quad d_e(\partial_\nu M^e)_j^{n+1} - d_c(\partial_\nu M^c)_j^{n+1} = \mu_e M_j^{e,*}(\partial_\nu u^e)_j^n, \tag{15b}$$

$$\forall P_j \in \tilde{\Gamma}, \quad P_m(M_j^{e,n+1} - M_j^{c,n+1}) = d_e(\partial_\nu M^e)_j^{n+1}, \tag{15c}$$

with a homogeneous Neumann condition on the boundary of the simulation box. This numerical scheme is similar to the scheme used in Kavian et al. (2014) for a static model of electric potential since there is no time derivative in the transmission condition of the discontinuity of M. Thus, we use the same fixed point method as in Kavian et al. (2014): starting from $M^k = M^n$, we solve

$$\forall \mathbf{i} \in [0, N]^3, \quad \frac{1}{\delta t} M_{\mathbf{i}}^{k+1} - d(\Delta M)_{\mathbf{i}}^{k+1} = \frac{1}{\delta t} M_{\mathbf{i}}^k, \tag{16a}$$

$$\forall P_j \in \tilde{\Gamma}, \quad d_e(\partial_\nu M^e)_j^{k+1} - d_c(\partial_\nu M^c)_j^{k+1} = \mu_e M_j^{e,*}(\partial_\nu u^e)_j^n, \tag{16b}$$

$$\forall P_j \in \tilde{\Gamma}, \quad P_m(M_j^{e,k+1} - M_j^{c,k}) = d_e(\partial_\nu M^e)_j^{k+1}, \tag{16c}$$

until the residual $\|M^{k+1} - M^k\|_{L^2(\Gamma)} / \|M^k\|_{L^2(\Gamma)}$ is inferior to 10^{-8}. Then we use M^{k+1} as the solution at the time t^{n+1}.

Remark 4.1. Between two pulse deliveries, it is not necessary to solve the equations on the potential, as well as the electrophoretic transport of M. It is then possible to use a much larger time step than the step used during the pulses.
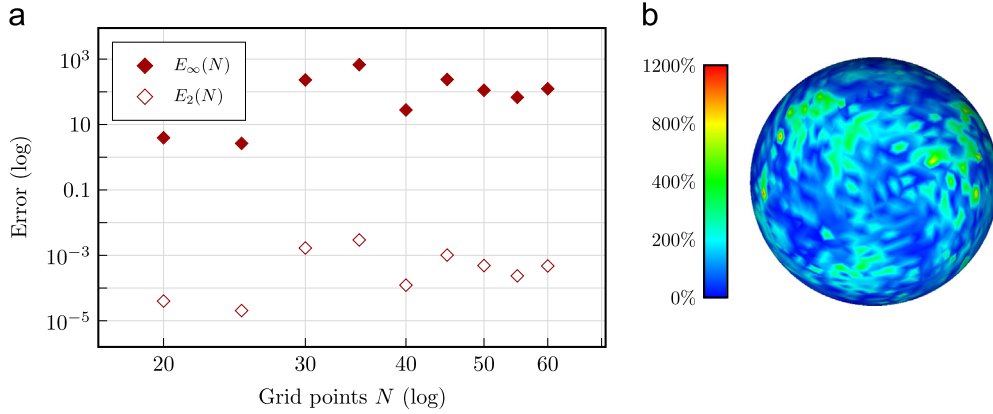
Fig. 3. (a) Non-convergence of the LBO discretization given by Xu (2004) on a sphere, using the intersection points between the cartesian grid and the level-set function. The error is defined in Eq. (18). (b) Spatial repartition of the error on the sphere with a 50^3 points wide cartesian grid.

4.2. Discretization of the reaction–diffusion model on the interface

In order to discretize Eq. (12k) on X_2, we will use the following numerical scheme:

$$\frac{1}{\delta t} X_2^{n+1} - d_L(\Delta_\Gamma) X_2^{n+1} = \frac{1}{\delta t} X_2^n + F_2(X_2^n, S_{ep}). \tag{17}$$

where $(\Delta_\Gamma) X_2^{n+1}$ is the approximation Laplace–Beltrami operator (LBO) Δ_Γ on the interface at time t^{n+1}.

4.2.1. Existing LBO discretizations

In Xu (2004), Xu reviewed several finite volumes methods to discretize the Laplace–Betrami operator. Most of them do not converge, but the author proposed two ways to compute the LBO on a smooth surface that converge under certain circumstances. We first applied the indirect discretization using an interpolation of the gradients (see Sections 3.1 and 4.1 of Xu, 2004), on a mesh generated with the intersection points that were defined in the previous section. Fig. 3 shows that no convergence is achieved, mainly due to the irregularities of the mesh. Indeed, whatever the pace of the cartesian grid, the intersection with a sphere always produces triangles with very heterogeneous dimensions.

Denoting by $\mathbf{\Psi}(\theta, \varphi)$ the parametrization of the sphere of radius R centered at the origin,

$$\mathbf{\Psi}(\theta, \varphi) = \begin{pmatrix} R \sin \varphi \sin \theta \\ R \cos \varphi \sin \theta \\ R \cos \theta \end{pmatrix}, \quad \forall (\theta, \varphi) \in [0, \pi] \times [0, 2\pi],$$

the curvature $\mathbf{H}$ is given by

$$\mathbf{H} = \Delta_\Gamma \mathbf{\Psi} = -\frac{2}{R} \nu,$$

and thus we compute an estimation of the coordinates, noted as ψ, from the given curvature. Remark that the solution $\mathbf{\Psi}$ is defined up to a constant, which is fixed by adding the relation $\psi(\theta, \varphi)/\epsilon = \mathbf{\Psi}(\theta, \varphi)/\epsilon$ on an arbitrary line of the discretization matrix, with ϵ being a small penalization parameter. We measure the convergence by computing

$$E_2 := \left\| \frac{|\psi - \mathbf{\Psi}|_2}{|\mathbf{\Psi}|_2} \right\|_{L^2(\Gamma)} \quad \text{and} \quad E_\infty := \left\| \frac{|\psi - \mathbf{\Psi}|_2}{|\mathbf{\Psi}|_2} \right\|_{L^\infty(\Gamma)}. \tag{18}$$

In a second time, we use a more regular mesh, generated by subdividing the faces of an icosaedron, so that all mesh triangles have similar dimensions and are nearly equilateral. The method then achieves a convergence of order almost 2, as shown in Fig. 4, but the spatial repartition of the error presents some oscillations that can degrade the solution of our diffusion problem.

4.2.2. LBO discretization for parametrized surfaces

Since a regular mesh is needed to improve convergence, and cells for *in vitro* experiments usually have a simple shape, we decided to directly express the LBO from a parametrization of the surface Γ.

Let $\theta \in]0, \pi[$ and $\varphi \in]0, 2\pi[$ and $\mathbf{\Psi}(\theta, \varphi)$ be this parametrization. The Riemanian metric at a point (θ, φ) is given by

$$g_{\theta\theta} := |\partial_\theta \mathbf{\Psi}(\theta, \varphi)|_2^2, \quad g_{\varphi\varphi} := |\partial_\varphi \mathbf{\Psi}(\theta, \varphi)|_2^2, \quad g_{\theta\varphi} := \langle \partial_\theta \mathbf{\Psi}(\theta, \varphi), \partial_\varphi \mathbf{\Psi}(\theta, \varphi) \rangle.$$

Let

$$\mathcal{G} := \begin{pmatrix} g_{\theta\theta} & g_{\theta\varphi} \\ g_{\theta\varphi} & g_{\varphi\varphi} \end{pmatrix}, \quad g := \det(\mathcal{G}) \quad \text{and} \quad \mathcal{G}^{-1} := \begin{pmatrix} g^{\theta\theta} & g^{\theta\varphi} \\ g^{\theta\varphi} & g^{\varphi\varphi} \end{pmatrix}.$$

The LBO is then given by

$$\Delta_\Gamma f(\theta, \varphi) = \frac{1}{\sqrt{|g|}} [\partial_\theta(\sqrt{|g|}(g^{\theta\theta} \partial_\theta f + g^{\theta\varphi} \partial_\varphi f)) \\ + \partial_\varphi(\sqrt{|g|}(g^{\theta\varphi} \partial_\theta f + g^{\varphi\varphi} \partial_\varphi f))]. \tag{19}$$

The interface is discretized by a cartesian grid in (θ, φ), with N_θ points in the θ-direction and $2N_\theta$ points in the φ-direction, so as the pace $\delta\theta$ is the same in both directions. For the sake of readability, we use the following notations:

$$\forall 0 \le k \le N_\theta, \quad \theta_k := \left(k + \frac{1}{2}\right) \delta\theta,$$

$$\forall 0 \le l \le 2N_\theta, \quad \varphi_l := \left(l + \frac{1}{2}\right) \delta\theta,$$

$$\tilde{g}_{kl} := \sqrt{|g(\theta_k, \varphi_l)|}, \quad g_{kl}^{\alpha\beta} = g^{\alpha\beta}(\theta_k, \varphi_l), \quad \forall (\alpha, \beta) \in \{\theta, \varphi\}.$$

The LBO is discretized using a centered second-order finite difference formula:

$$(\Delta_\Gamma f)_{kl} = \frac{1}{\tilde{g}_{kl}} \left[\frac{\tilde{g}_{k+(1/2)l} g_{k+(1/2)l}^{\theta\theta}(f_{k+1l} - f_{kl}) - \tilde{g}_{k-(1/2)l} g_{k-(1/2)l}^{\theta\theta}(f_{kl} - f_{k-1l})}{\delta\theta^2} \right.$$
$$+ \frac{\tilde{g}_{kl+(1/2)} g_{kl+(1/2)}^{\varphi\varphi}(f_{kl+1} - f_{kl}) - \tilde{g}_{kl-(1/2)} g_{kl-(1/2)}^{\varphi\varphi}(f_{kl} - f_{kl-1})}{\delta\theta^2}$$
$$+ \frac{\tilde{g}_{k+1l} g_{k+1l}^{\theta\varphi}(f_{k+1l+1} - f_{k+1l-1}) - \tilde{g}_{k-1l} g_{k-1l}^{\theta\varphi}(f_{k-1l+1} - f_{k-1l-1})}{4\delta\theta^2}$$
$$\left. + \frac{\tilde{g}_{kl+1} g_{kl+1}^{\theta\varphi}(f_{k+1l+1} - f_{k-1l+1}) - \tilde{g}_{kl-1} g_{kl-1}^{\theta\varphi}(f_{k+1l-1} - f_{k-1l-1})}{4\delta\theta^2} \right]. \tag{20}$$

The following periodicity conditions are used:

$$f_{k, 2N_\theta + 1} = f_{k, 0}, \quad f_{k, -1} = f_{k, 2N_\theta},$$
$$f_{-1, l} = f_{0, (l + N_\theta)[N_\theta]}, \quad f_{N_\theta + 1, l} = f_{N_\theta, (l + N_\theta)[N_\theta]}.$$
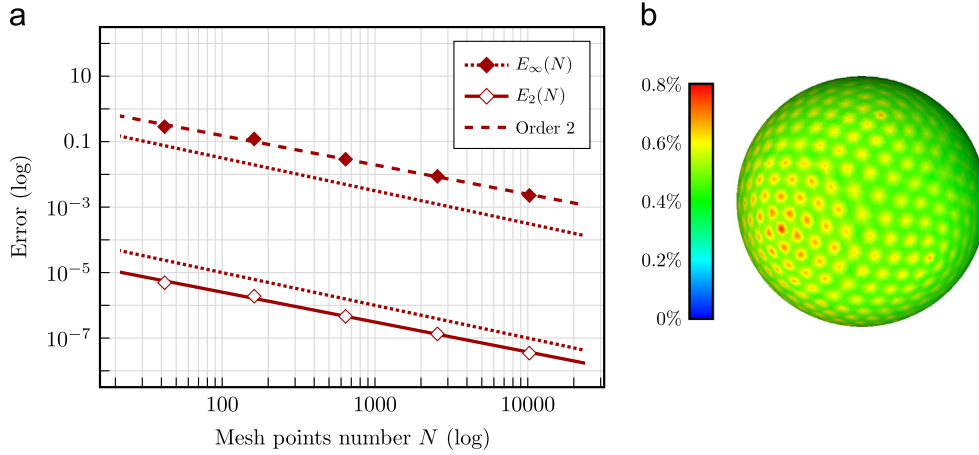
Fig. 4. Convergence (a) and spatial repartition of the error (b) using a regular mesh of a sphere. This mesh is generated by subdividing the faces of an icosahedron and projecting the vertices on the sphere.
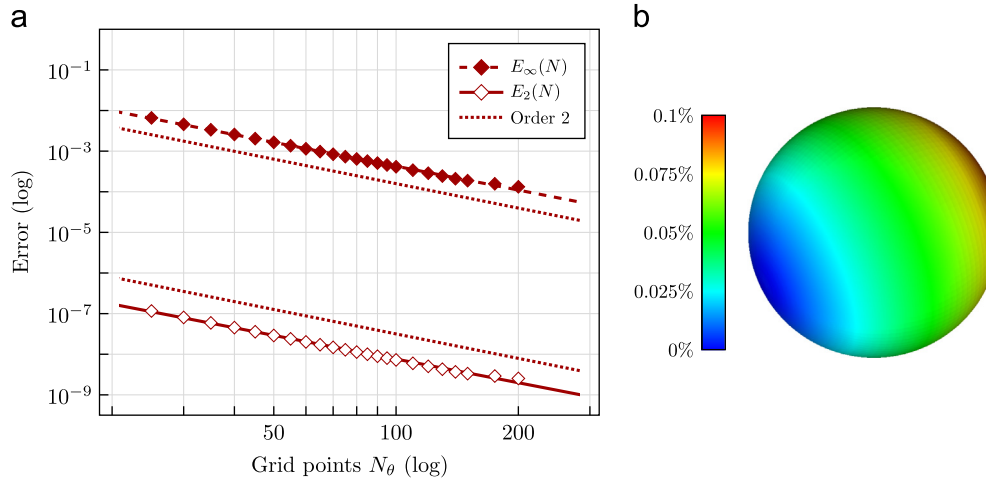
Fig. 5. (a) Convergence of (θ, φ)-LBO-discretization on a sphere. The error is computed by Eq. (18). (b) Spatial repartition of the error.

Note that the metric has to be computed halfway between grid points, in particular at the poles $\theta = 0$ and $\theta = \pi$. Usually, $\mathcal{G}$ is not invertible at these points, and the LBO cannot be defined using the parametrization. In that case, we compute the metric with $\theta = \epsilon$ or $\theta = \pi - \epsilon$, with ϵ being $\sim 10^{-40}$.

In order to validate our spatial discretization of the LBO, here again we compute the curvature of a sphere. Moreover, we test our discretization on an ellipsoid, whose parametrization is given by

$$\Psi(\theta, \varphi) = \begin{pmatrix} r \sin \theta \cos \varphi \\ r \sin \theta \sin \varphi \\ \alpha r \cos \theta \end{pmatrix}, \quad \alpha \neq 0,$$

and the curvature by

$$H = \Delta_\Gamma \Psi(\theta, \varphi) = -\frac{\alpha}{r} \frac{1 + \cos^2 \theta + \alpha^2 \sin^2 \theta}{(\cos^2 \theta + \alpha^2 \sin^2 \theta)^2} \begin{pmatrix} \alpha \sin \theta \cos \varphi \\ \alpha \sin \theta \sin \varphi \\ \cos \theta \end{pmatrix}.$$

Convergence results for the finite difference method are presented in Figs. 5 and 6: as expected, the order 2 of convergence is achieved. Compared to the finite volume methods presented by Xu, we obtain a better convergence, as well as a significant

improvement in computation time, the drawback being that we need an analytical expression of the surface.

4.3. Coupling the discretizations

In the previous paragraphs, we presented two different ways to describe the interface. Since these two sets of points do not coincide (see Fig. 7), we need to perform interpolations between them: once step (13) has been performed, X_2 must be computed on the (θ, φ)-grid to continue on step (17), and the reverse operation has to be done after this diffusion step. In this paragraph, we will designate by *intersection points* the locations of the intersections between the 3D cartesian grid (representing $\mathcal{O}_c \cup \mathcal{O}_e$) and Γ. The points defined by the (θ, φ)-grid involved in the LBO discretization will be called *mesh points*.

4.3.1. From the mesh points to the intersection points

To obtain the values on the intersection points knowing the function on the mesh points, the coordinates of the intersection points are directly projected on the (θ, φ)-grid. This can be done straightforwardly if the expression of the reciprocal parametrization is known. A regular bilinear interpolation is then possible on
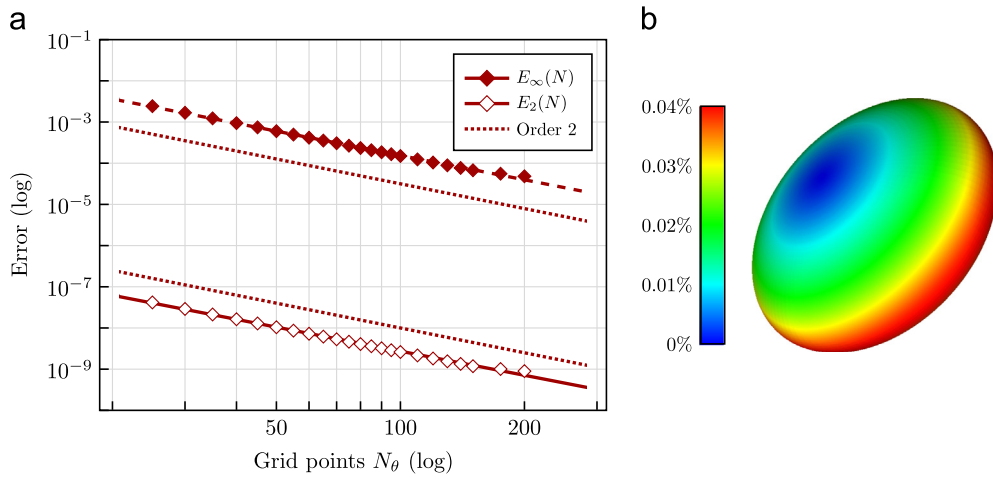
Fig. 6. (a) Convergence of the (θ, φ)-LBO-discretization on an ellipsoid ($\alpha = 0.5$). The error is computed by Eq. (18). (b) Spatial repartition of the error.
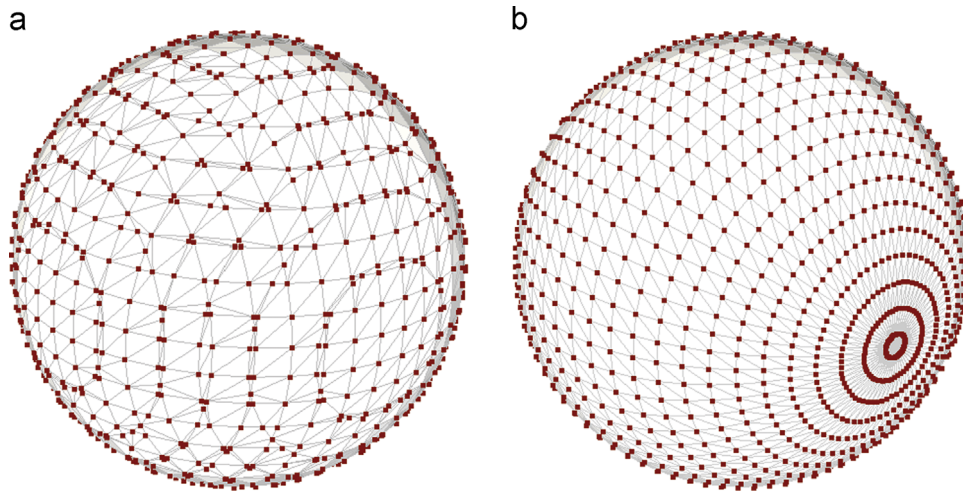
Fig. 7. (a) Mesh generated from the intersection points with the cartesian grid, used for the resolution of the potential and transport equations. (b) (θ, φ)-mesh on which the LBO is discretized.

this grid: if (θ_j, φ_j) are the coordinates of the point $P_j \in \tilde{\Gamma}$ in $[\theta_k, \theta_{k+1}] \times [\varphi_l, \varphi_{l+1}]$:

$$f(\theta_j, \varphi_j) \sim (f_{kl} - f_{k+1l} - f_{kl+1} + f_{k+1l+1}) \frac{(\theta_j - \theta_k)(\varphi_j - \varphi_l)}{d\theta^2}$$

$$+ (f_{k+1l} - f_{kl}) \frac{\theta_j - \theta_k}{d\theta} + (f_{kl+1} - f_{kl}) \frac{\varphi_j - \varphi_l}{d\theta} + f_{kl}.$$

4.3.2. From the intersection points to the mesh points

For the reverse interpolation, we consider the 3D-cartesian cell in which is located a mesh point. In this cell, the interface is described by a convex polygon whose vertices are intersection points where values are known (see Fig. 8). We use barycentric coordinates to perform the interpolation on the mesh point, as given by Meyer et al. (2002). Let $P_j, j = 1, \dots, j_{\max}$ be the list of these vertices, ordered along j around the mesh point P_{kl}. We define the weights

$$\alpha_j = \frac{\cotan(\vec{P_j P_{kl}}, \vec{P_j P_{j-1}}) + \cotan(\vec{P_j P_{kl}}, \vec{P_j P_{j+1}})}{|\vec{P_{kl} P_j}|_2^2}.$$

The value of a function f at P_{kl} is then given by $\sum_{i=1}^{j_{\max}} \alpha_j f_j$.

Fig. 9 shows that the two interpolation methods are of order 2.
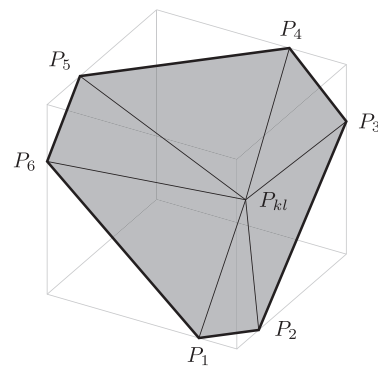
Fig. 8. Interpolating values known on the intersection points $P_j, j = 1:6$ to evaluate a function at the mesh point P_{kl}.

5. Results

In order to run the simulations, we need to adjust the parameters of the equations. Parameters for the electric potential can be fixed in accordance with the papers of Neu et al. Moreover, the diffusion of lipids along the membrane is quite well-known, and of order $1\ \mu m^2/s$ and the time constants $\tau_{2,\mathrm{perm}}$ and $\tau_{2,\mathrm{res}}$ can be obtained by the experiments. It thus remains to choose the
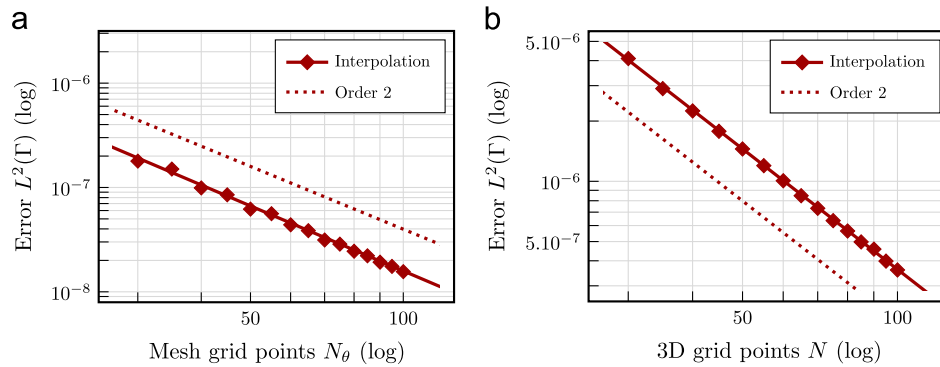
Fig. 9. Convergence of interpolation methods for the mapping $(x, y, z) \mapsto x^2 + 1$. The computed error is the $L^2(\Gamma)$ norm of the relative difference between the interpolation and the solution: (a) from the mesh points to the intersection points. (b) From the intersection points to the mesh points.

4 parameters of the sigmoidal functions β_1 and β_2 as well as the values of the permeabilities P_1 and P_2. Since it is not the scope of the present paper to calibrate precisely the model with some specific experiments, we choose parameters that provide results that are qualitatively in accordance with the experiments. All the parameters are given in Table 1. We emphasize that a precise calibration of the model would be necessary to obtain quantitative results, however this represents a huge amount of work: it needs the development of specific numerical tools and appropriate experimental data to fit with and it is far beyond the scope of the present paper.

5.1. Diffusion and transport of molecules in a 2D cell, without lipid diffusion

In order to validate our model, we first confront both the numerical transport and the diffusion of the molecule to the experimental results of PI uptake for various pulses. Based on the articles of Escoffre et al. (2011) and DeBruin and Krassowska (1999), we choose the parameters for the simulations given by Table 1.[2] We compare the results of the simulation with the experimental data of Escoffre et al. (2011) involving millipulses. Comparison is also led with the observations of Vernier et al. (2003), using micro- and nanopulses. In these 2D simulations, we omit the surface diffusion of lipids on the cell membrane.

For long duration pulses, the electrophoretic effect brings more PI on the part of the cell which faces the anode. This accumulation leads to an asymmetry in the PI repartition inside the cytosol. Figs. 10 and 11 show that the modeling is in good agreement with the experiments, at least qualitatively.

5.2. Simulating the whole model in a 3D cell

It has been very recently reported in Silve et al. (2014) that, strikingly, for the same number of pulses, a high frequency rate of repetition is less efficient than pulses repeated at low frequency. From the modeling point of view, this question of such "desensitization" has never been addressed and we show in this section that our model can provide an explanation to these observations.

We performed 3D-simulations of a spherical cell submitted to 10 permeabilizing micropulses (10 μs, 40 kV/m), with various repetition rates from 1 to 1000 Hz. In these simulations, we set the

Table 1
Simulation parameters. Biological parameters are taken from DeBruin and Krassowska (1999) and Escoffre et al. (2011).

Variable	Symbol	Value	Unit (SI)
Biological parameters			
Spherical cell radius	r	8×10^{-6}	m
Extracellular conductivity	σ_e	5	S m^{-1}
Intracellular conductivity	σ_c	0.455	S m^{-1}
Capacitance	C_m	9.5×10^{-3}	F m^{-2}
Membrane surface conductivity	S_0	1.9	S m^{-2}
Resting potential	u_0	-40×10^{-3}	V
Molecule diffusion in cytosol	d_c	10^{-9}	m^2 s^{-1}
Molecule diffusion in outer medium	d_e	10^{-8}	m^2 s^{-1}
Molecule motility in outer medium	μ_e	10^{-6}	m^2 V^{-1} s^{-1}
Model parameters for X_1			
Pore conductivity	S_1	1.1×10^6	S m^{-2}
Pore permeability	P_1	10^{-6}	m s^{-1}
Poration threshold	V_{th}	0.2	V
Poration switch speed	k_1	40	V^{-1}
Poration characteristic time	τ_1	2×10^{-5}	s
Model parameters for X_2			
Altered membrane conductivity	S_2	10^3	S m^{-2}
Altered membrane permeability	P_2	10^{-7}	m s^{-1}
Conductivity threshold	$X_{1,th}$	8×10^4	S m^{-2}
Permeabilization switch speed	k_2	10	S^{-1} m^2
Permeabilization dynamic	$\tau_{2,perm}$	10^{-6}	s
Membrane recovery time	$\tau_{2,res}$	60	s

diffusion of the lipids on the membrane to

$$d_L = 10^{-12} \text{ m}^2 \text{ s}^{-1}.$$

The average permeabilization P_m of the membrane, as well as the concentration of molecules that entered the cell, are measured along time.

Fig. 12 shows the distribution of P_m on the surface of the cell at different instants of the 1 Hz and 1000 Hz simulations. A comparative animation of these two simulations is also available as Supplementary Material. We see that in the case of a fast repetition rate, the altered lipids do not have time to be evenly spread on the membrane. Since the next pulse will alter the same region as the first, the total quantity of altered lipids will be lower than the 1 Hz case.

Fig. 13 presents the average of P_m after each pulse. As expected, the permeabilization is more efficient if enough time is left between pulses to let the lipids diffuse.

In Fig. 14, we plot the average concentration of molecules in the cytoplasm along time, growing as long as the value P_m is non-zero. We can see that the 1000 Hz case leads to a lower efficiency of the permeabilization leading to a lower amount of internalized molecules. We emphasize on the fact that the final quantity of molecules is highly dependent on the constants $\tau_{2,res}$ and P_2. If P_2

---

[2] Since the time scales are from a few microseconds for the poration to a few hour for the total recovery of the membrane, the computation times are very huge. Since our goal is to provide qualitative behaviours of the model, and not quantitative results, for the sake of simplicity we decrease to 60 s the time recovery of the membrane by exocytosis. Forthcoming works of parallel computing will be addressed to fit quantitatively the model with the biological data.

a

b

Fig. 10. PI uptake during 10 millipulses of 20 ms, 50 kV/m, 1 Hz. Comparison between the experiments (a), as given by Escoffre et al. (2011) and the simulation (b). PI concentrations are given relative to the external initial concentration. Two different color scales are used to represent PI concentration, since the proportion of PI inside the cell is much lower than outside. (For interpretation of the references to color in this figure caption, the reader is referred to the web version of this paper.)

a

b
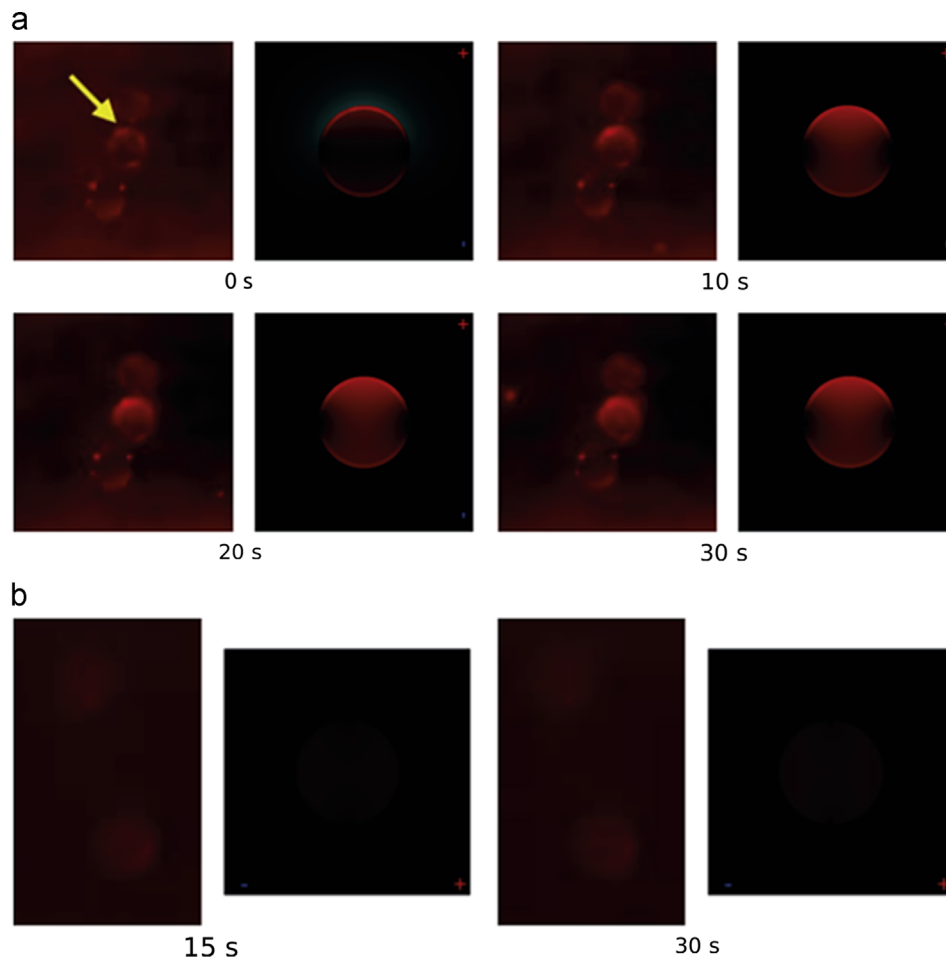
Fig. 11. Comparison between simulations and experiences from Vernier et al. (2003). The time indications are taken after all pulses are applied. (a) 5 micropulses of 100 μs, 500 kV/m, 4 Hz. (b) 10 nanopulses of 30 ns, 2.5 MV/m, 4 Hz. The color scale is the same as in Fig. 10. (For interpretation of the references to color in this figure caption, the reader is referred to the web version of this paper.)

is large enough (for example for very small molecules), the concentration can reach its maximum value in a very short time whatever the pulse frequency. On the contrary, small values of P_m increase the difference between the final internalized quantity of molecules. In particular, these simulations corroborate results of High Voltage/Low Voltage experiments (Šatkauskas et al., 2005) that, within the first seconds after the pulses, show a better permeabilization to DNA when the lapse of time between pulses is longer.

6. Conclusion

We have presented a model, which describes simultaneously the conducting and the permeable states of the membrane, without identifying these states. This is an important novelty in the modeling of cell electropermeabilization, which only dealt with the electrical behaviour of the membrane before. Our model makes it possible to compare straightforwardly the majority of the available experimental data, which essentially deal with the
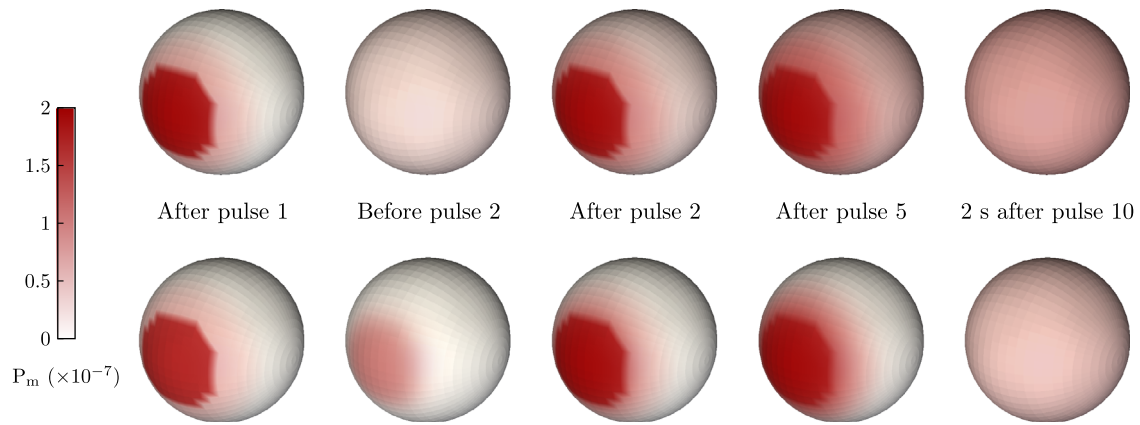
Fig. 12. Influence of the pulse frequency on the membrane permeabilization P_m. The magnitude of each pulse is 40 kV/m during 10 μs. 10 pulses are applied on both cells, but the time between pulses is different: 1 s for the top line, 1 ms for the bottom line. After 10 pulses, the average of P_m is around 8×10^{-8} for the 1 Hz case, and half for the 1000 Hz case. An animation of these simulation is available as Supplementary Content.
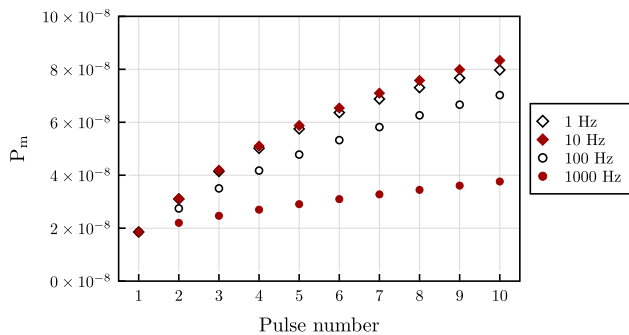
Fig. 13. Average permeabilization P_m on the cell after each of the 10 pulses of Fig. 12 for different pulse repetition rates.
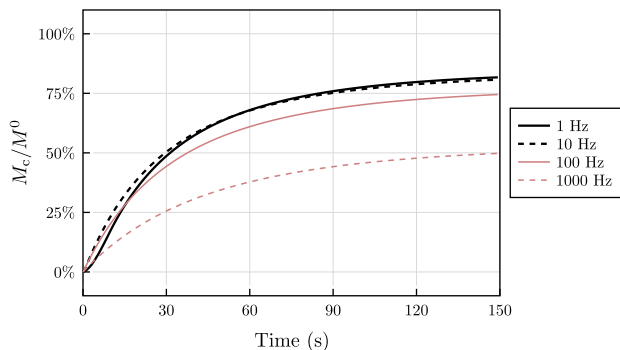
Fig. 14. Average concentration M_c inside the cell for different pulse repetition rates, expressed as a percentage of external concentration M^0. As in Figs. 12 and 13, 10 micropulses (40 kV/m during 10 μs each) are applied at different frequencies.

diffusion of non-permeant molecules across the membrane, taking into account the fast time to recover a low conductivity and the long-time permeabilized state. Another important feature of our model is that the diffusion of the lipids along the membrane makes it possible to explain the striking experimental observations: the more you wait between the pulse, the more efficient is the permeabilization, which cannot be accounted for by considering the membrane conductivity only.

Therefore our numerical results show that the model behaves qualitatively in accordance with the experiments. In order to provide quantitative results, forthcoming work will be to calibrate the parameters. We emphasize that our model was built with the least parameters as possible in order to solve the inverse problem of the fitting.

Appendix A. Supplementary material

Supplementary data associated with this paper can be found in the online version at http://dx.doi.org/10.1016/j.jtbi.2014.06.027.

References

Benz, R., Beckers, F., Zimmermann, U., 1979. Reversible electrical breakdown of lipid bilayer membranes: a charge pulse relaxation study. J. Membr. Biol. 48 (2), 181–204, http://dx.doi.org/10.1007/BF01872858.

Chapuis, R., Aubertin, M., 2003. On the use of the Kozeny–Carman equation to predict the hydraulic conductivity of soils. Can. Geotech. J. 40 (3), 616–628, http://dx.doi.org/10.1139/t03-013.

Chen, Y., Lagerholm, B., Yang, B., Jacobson, K., 2006. Methods to measure the lateral diffusion of membrane lipids and proteins. Methods 39 (2), 147–153, http://dx.doi.org/10.1016/j.ymeth.2006.05.008.

DeBruin, K., Krassowska, W., 1999. Modelling electroporation in a single cell. I. Effects of field strength and rest potential. Biophys. J. 77 (3), 1213–1224, http://dx.doi.org/10.1016/S0006-3495(99)76973-0.

Escoffre, J., Portet, T., Favard, C., Teissié, J., Dean, D., Rols, M., 2011. Electromediated formation of DNA complexes with cell membranes and its consequences for gene delivery. Biochim. Biophys. Acta Biomembr. 1808 (6), 1538–1543, http://dx.doi.org/10.1016/j.bbamem.2010.10.009.

Glogauer, M., Lee, W., McCulloch, C., 1993. Induced endocytosis in human fibroblasts by electrical fields. Exp. Cell Res. 208 (1), 232–240, http://dx.doi.org/10.1006/excr.1993.1242.

Harakawa, S., Inoue, N., Hori, T., Tochio, K., Kariya, T., Takahashi, K., Doge, F., Suzuki, H., Nagasawa, H., 2005. Effects of a 50 Hz electric field on plasma lipid peroxide level and antioxidant activity in rats. Bioelectromagnetics 26 (7), 589–594, http://dx.doi.org/10.1002/bem.20137.

Kargol, M., 1996. A more general form of Kedem and Katchalsky's practical equations. J. Biol. Phys. 22 (1), 15–26, http://dx.doi.org/10.1007/BF00383819.

Kavian, O., Leguèbe, M., Poignard, C., Weynans, L., 2014. "Classical" electropermeabilization modeling at the cell scale. J. Math. Biol. 68 (1–2), 235–265, http://dx.doi.org/10.1007/s00285-012-0629-3.

Leguèbe, M., Poignard, C., Weynans, L., 2013. A Second-Order Cartesian Method for the Simulation of Electropermeabilization Cell Models. Research Report RR-8302, INRIA, URL: ⟨http://hal.inria.fr/hal-00821758⟩.

Meyer, M., Barr, A., Lee, H., Desbrun, M., 2002. Generalized barycentric coordinates on irregular polygons. J. Graph. Tools 7 (1), 13–22, http://dx.doi.org/10.1080/10867651.2002.10487551.

Neu, J., Krassowska, W., 1999. Asymptotic model of electroporation. Phys. Rev. E 53 (3), 3471–3482, http://dx.doi.org/10.1103/PhysRevE.59.3471.

Neu, J., Krassowska, W., 2006. Singular perturbation analysis of the pore creation transient. Phys. Rev. E 74 (031917), 1–9, http://dx.doi.org/10.1103/PhysRevE.74.031917.

Nikolova, B., Georgieva, M., Savu, D., Tsoneva, I., 2012. Cell membrane alteration by weak alternating electric field at low frequency. Rom. Rep. Phys. 64 (4), 1046–1052.

Poignard, C., Silve, A., Campion, F., Mir, L., Saut, O., Schwartz, L., 2011. Ion flux, transmembrane potential, and osmotic stabilization: a new electrophysiological dynamic model for eukaryotic cells. Eur. Biophys. J. 40 (3), 235–246, http://dx.doi.org/10.1007/s00249-010-0641-8.

Rols, M., Delteil, C., Golzio, M., Teissié, J., 1998. Control by ATP and ADP of voltage-induced mammalian-cell-membrane permeabilization, gene transfer and resulting expression. Eur. J. Biochem. 254 (2), 382–388, http://dx.doi.org/10.1046/j.1432-1327.1998.2540382.x.

Silve, A., Guimerà Brunet, A., Al-Sakere, B., Ivorra, A., Mir, L., 2014. Comparison of the effects of the repetition rate between microsecond and nanosecond pulses: electropermeabilization-induced electro-desensitization? Biochim. Biophys. Acta 840 (7), 2139–2151 http://dx.doi.org/10.1016/j.bbagen.2014.02.011 ⟨URL http://www.sciencedirect.com/science/article/pii/S0304416514000725⟩.

Smith, K., Weaver, J., 2012. Electrodiffusion of molecules in aqueous media: a robust, discretized description for electroporation and other transport phenomena. IEEE Trans. Bio-med. Eng. 59 (6), 1514–1522, http://dx.doi.org/10.1109/TBME.2011.2180378.

Smith, K., Neu, J., Krassowska, W., 2004. Model of creation and evolution of stable electropores for DNA delivery. Biophys. J. 86 (5), 2813–2826, http://dx.doi.org/10.1016/S0006-3495(04)74334-9.

Šatkauskas, S., André, F., Bureau, M., Scherman, D., Miklavčič, D., Mir, L., 2005. Electrophoretic component of electric pulses determines the efficacy of in vivo DNA electrotransfer. Hum. Gene Ther. 16 (10), 1194–1201, http://dx.doi.org/10.1089/hum.2005.16.1194.

Tarek, M., 2005. Membrane electroporation: a molecular dynamics simulation. Biophys. J. 88 (6), 4045–4053, http://dx.doi.org/10.1529/biophysj.104.050617.

Teissié, J., Ramos, C., 1998. Correlation between electric field pulse induced long-lived permeabilization and fusogenicity in cell membranes. Biophys. J. 74 (4), 1889–1898 http://dx.doi.org/10.1016/S0006-3495(98)77898-1.

Tieleman, D., 2004. The molecular bases of electroporation. BMC Biochem. 5 (10), 1–12, http://dx.doi.org/10.1186/1471-2091-5-10.

Tocanne, J.-F., Dupou-Cézanne, L., Lopez, A., 1994. Lateral diffusion of lipids in model and natural membranes. Prog. Lipid Res. 33 (3), 203–237, http://dx.doi.org/10.1016/0163-7827(94)90027-2.

Vaz, W., Goodsaid-Zalduondo, F., Jacobson, K., 1984. Lateral diffusion of lipids and proteins in bilayer membranes. FEBS Lett. 174 (2), 199–207, http://dx.doi.org/10.1016/0014-5793(84)81157-6.

Vernier, T., Sun, Y., Marcu, L., Salemi, S., Craft, C., Gundersen, M., 2003. Calcium bursts induced by nanosecond electric pulses. Biochem. Biophys. Res. Commun. 310 (2), 286–295, http://dx.doi.org/10.1016/j.bbrc.2003.08.140.

Xu, G., 2004. Discrete Laplace–Beltrami operators and their convergence. Comput. Aided Geom. Des. 21 (8), 767–784, http://dx.doi.org/10.1016/j.cagd.2004.07.007.